ISSN No:-2456-2165

Unsteady Mixed Convective Flow of Casson Nanofluid in a Darcy-Forchheimer Medium with Slip and Temperature Jump Condition

O.A. Ajala[1]; S.D. Ogundiran[1*]; S.O. Salawu[2]
[1]Department of Pure and Applied Mathematics, Ladoke Akintola University of Technology, Ogbomoso, Nigeria
[2]Department of Mathematics, Bowen University, Iwo, Nigeria

Corresponding Author:- S.D. Ogundiran[1*]

Abstract:- Sequel to the need to improve output, there is a growing demand to optimize the thermal conductivity and proficiency of industrial-based fluids. Consequently, viscous non-Newtonian fluids carrying nanoparticles may be utilized as a material to satisfy engineering and industrial demands for increased productivity. This may be applicable to electronic devices, technological devices, biomedical sciences, and other fields. As a result, this work examined unsteady mixed convective flow of Casson nanofluid in a non-Darcy channel with slip and temperature jump constraints. Shooting approach and fourth-order Runge-Kutta method were used to provide the solution to the dimensionless formulated model. Examined are the effects of the ingrained relevant dynamical terms on the flow characteristics, and graphs and tabular presentations of the calculated outcomes are used to elucidate the findings. The study's findings showed that the diffusion of small particles into a fluid boosted thermal conductivity. In addition, the flow rate decreased as the Hartmann number and Forchheimer dynamical term increased. The findings of this study have applications in manufacturing, engineering, and other fields of sciences and technologies.

Keywords:- *Casson Nanofluid; Darcy-Forchheimer Medium; Mixed Convection; Temperature Jump; Unsteady; Velocity Slip.*

I. INTRODUCTION

Researchers in the fields of science and engineering with a focus on fluids that increase heat and mass have paid great attention to the development of a novel type of fluid known as nanofluids in recent decades of interesting and progressive research [1]. [2] has found that the use of nanoparticles enhances the fluid's thermophysical properties and significantly increases heat transmission. The ideal rate of development in this subject has gained increased attention as a result of the utility of nanotechnology in many manufacturing and production sectors, including engineering, energy technologies, and medicine, as stated by [3]. Using a horizontal perforated sheet that linearly contracts and expands in response to mass transpiration, researchers [4] examined the flow of a Casson flowing with electrical conductance within a laminar boundary layer. The flow was also subjected to circumstances of Navier's slip and second-order slip in the presence transverse magnetic field applied in the system. The non-Newtonian flow under study follows the Casson model-driven flow's rheological equation. By making use of the proper similarity transformations, the partial differential equations regulating the boundary layer flow were analytically represented and reduced to a nonlinear boundary value problem in ordinary differential equations. The sensitivity parameters were discovered to be functions of the similarity solution. Such a solution was either unique, or dual solutions exist in a region defined by the mass transfer induced slip parameter. The results obtained show that an increase in the magnetic parameter resulting in expansion of the unique solution region and contraction of the dual solution region for the flow due to the induced Lorentz force. In the unique solution region, an increase in magnitudes of mass suction induced slip and the first/second-order slip parameters result in a reduction of the wall shear stress in the shrinking sheet, while the wall shear stress with mass suction increases with the Casson and the magnetic effects. [5] Investigated motion of temperature dependent viscosity and thermal conductivity of steady incompressible laminar free convective (MHD) non-Newtonian Casson fluid flow over an exponentially stretching surface with exponentially decaying internal heat generation, slip flow and convective heating condition. It was assumed that natural convection is induced by buoyancy and exponentially decaying internal heat generation across the space with convective boundary and velocity slip. The derived ordinary differential equations were solved numerically using the MATLAB bvp4c solver. A parametric study was performed to illustrate the influence of Prandtl number, Casson parameter, temperature dependent viscosity, temperature dependent thermal conductivity, Magnetic parameter , biot number and velocity slip on the fluid velocity and temperature profiles within the boundary layer. The flow controlling parameters were found to have a great effect on the resulting flow profiles. [6] Examined casson fluid flow over a vertical porous surface with chemical reaction in the presence of magnetic field. Similarity analysis was used to transform the system of partial differential equations reducing the flow problem into ordinary differential equations. The reduced system of equations was solved using the Newton Raphson shooting method alongside the Fourth-order Runge-Kutta algorithm.

The results were presented graphically and in tabular form for various controlling parameters.

A research on convective transport in nanofluids where some slip mechanisms capable of producing a relative velocity between the base fluid and the nanoparticles were considered and only Brownian diffusion and thermophoresis were found to be the important ones. It was also observed that nanoparticles move homogeneously with the fluid in the presence of eddies which are turbulent were considered by [7]. [8] Investigated the effects of viscous dissipation, suction, thermal diffusion and thermal radiation on the boundary layer flow of nanofluids over a permeable moving flat plate. Runge-Kutta-Fehberg method with the shooting technique was employed as a numerical method for the analysis. A comparative study of the results obtained with previously published work in a limiting sense showed a viable agreement. The boundary layer flow of nanofluid over an unsteady stretching surface in the presence of thermal radiation was examined by [9]. Shooting method with Runge- Kutta-Fehberg scheme was used to numerically analyse the flow scenario. The heat transfer rate at the surface was observed to increase with an increase in the Brownian motion but reduce for thermophoresis. [10] Studied hydromagnetic transport phenomena from a stretching or shrinking nonlinear nanomaterial sheet with Navier slip and convective heating: a model for bio-nano-materials processing. The transformed equations were solved using Runge-Kutta-Fehberg fourth fifth order implemented on Maple software and the result depicted that the magnetic parameter reduced the velocity but enhanced the temperature. [11] Worked on the effects of nanoparticles on non-Darcy mixed convective transfer of heat within nanofluids over a stretching and shrinking wedge. A solution to the equations of the flow was obtained using fourth order Runge-Kuttamethod along with shooting technique. The result showed that friction factor reduced with an increase in the nanoparticle concentration while the rate of heat transfer increased with it. [12] analysed the computational analysis for bio-convection of microorganisms in Prandtl nanofluid Darcy-Forchheimer flow across an inclined sheet. Runge-Kutta method alongside shooting technique were used to obtain the solution which revealed that the velocity declined with an increase in the porosity parameter. [13] Embarked on a numerical study of flow and heat transfer of a nanofluid past a vertical cone. The obtained equations were solved by Galerkin method with the basis of Legendre functions. Using higher values of volume fraction led to an enhancement of the mechanical behaviour at the surface of the fluid, thereby enhancing the cooling process within the flow. A numerical studied of Casson nanofluid past horizontal stretching surface with magnetic effect and Joule heating was presented by [14]. Slip and thermal convective boundary conditions are considered in the study. A numerical technique of Keller box is applied to the nonlinear ODEs which are obtained by applying the similarity transformation to the nonlinear partial differential equations. The magnetic field and Joule heating effects were observed graphically. It was noted that Nusselt number declines whereas Sherwood number rises by increasing Eckert number. The impact of increasing Hartman number resulted in the decrease of both Sherwood and Nusselt number. The combined effects of Dufour and Soret on the heat and mass transfer in a Casson nanofluid flow over an unsteady stretching sheet with thermal radiation and heat generation. The effects of partial slip on the velocity at the boundary, convective thermal boundary condition, and Brownian and thermophoresis diffusion coefficients on the concentration boundary condition were investigated by [15]. The model equations were solved using the spectral relaxation method. The results show that the fluid flow, temperature and concentration profiles were significantly influenced by the fluid unsteadiness, the Casson parameter, magnetic parameter and the velocity slip. The effect of increasing the Casson parameter was to suppress the velocity and temperature growth. An increase in the Dufour parameter reduces the flow temperature, while an increase in the value of the Soret parameter causes increase in the concentration of the fluid. Again, increasing the velocity slip parameter reduces the velocity profile whereas increasing the heat generation parameter increases the temperature profile. A validation of the work is presented by comparing the current results with existing literature.

The effects of combined variable viscosity and thermal conductivity, nonlinear radiation and non-Darcian porous medium on a boundary layer MHD Casson nanofluid flow over a vertical flat plate with convective heating and velocity slip boundary conditions was investigated by [16]. The governing transport nonlinear partial differential equations and the boundary conditions were non-dimensionalized. The resulting system of coupled partial differential equations is then reduced to a set of coupled nonlinear ordinary differential equations using similarity transformation. Galerkin weighted residual method (GWRM) was then employed to solve the resulting set of equations. Numerical results were obtained for dimensionless velocity, temperature and nanoparticle volume fraction (nanoparticle concentration). It was found that the velocity increases, while both temperature and nanoparticle volume fraction decrease with increased values of variable thermal conductivity and viscosity. Comparisons were carried out with published data in the literature thereby validating the numerical results. An excellent agreement is observed. Furthermore, this present study can find applications in the process involving nanofluid operations. [17] Studied how to develop a dynamical system for the magnetohydrodynamic (MHD) flow of an electrically conducting Casson nanofluid on exponentially shrinking and stretching surfaces, in the presence of a velocity and concentration slip effect, with convective boundary conditions. The results revealed that the temperature of the fluid increases with the extended values of the thermophoresis parameter, the Brownian motion parameter, and the Hartmann and Biot numbers, for both solutions. The presence of dual solutions depends on the suction parameter. In order to indicate that the first solution is physically relevant and stable, a stability analysis had been performed. [19] Examined MHD Boundary Layer Flow Past an Exponentially Stretching Sheet with Darcy-Forchheimer

Flow showed that the rate of heat transfer increased with an increase in the permeability parameter.

[24] Studied natural convective non-Newtonian Casson fluid flow in a porous medium with slip and temperature boundary conditions. Inspired by the aforementioned research, we attempted to examine unsteady mixed convective flow of Casson nanofluid in a Darcy-Forchheimer channel with slip and temperature jump boundary conditions in this work. In this study, the motion of nanoparticles in a fluid flow was taken into account along with thermophoresis and Brownian motion. This study's innovation is the way relevant parameters affect mixed convective flow of Casson nanofluid in a non-Darcy medium under slip and temperature jump conditions. Using the shooting scheme alongside fourth-order Runge Kutta method, the derived non-linear ordinary differential equations were solved. The numerical findings for velocity, temperature and concentration are presented in plots. The findings of this study make a substantial contribution to our knowledge and complement earlier research for applications in fields like biomedical engineering and heat transfer.

II. FORMULATION OF THE PROBLEM

Examine a combined current-driven non-compressible, current conducting, and hydromagnetic Casson nanofluid flow in a vertically permeable channel. The fluid was set in motion by the steady, periodic heating of the plates, which caused a gradient in the fluid's temperature and concentration. Based on this supposition, suction was applied to one porous plate (y = -h) while injection was applied to the other porous plate (y = +h). Slip and a temperature spike heated the low wall. At y = h, the porous plate was lifted vertically and parallel to the x-axis.

For Casson fluid, the constituting equations of isotropic and oscillatory flow can be expressed as [21, 22 ,23].

$$\tau_{ij} = \begin{cases} \left(\mu_B + P_y / \sqrt{2\pi_c}\right) 2e_{ij}, & \pi_c > \pi \\ \left(\mu_B + P_y / \sqrt{2\pi}\right) 2e_{ij}, & \pi > \pi_c \end{cases} \tag{1}$$

τ_{ij} is the $(i,j)^{th}$ stress tensor constituent, e_{ij} is the $(i,j)^{th}$ strain rate tensor constituent , $\pi = e_{ij}^2$ represents the product of the constituent of the strain rate tensor, π_c is the threshold value of this product dependent upon the Shear-thinning fluid, μ_B is the deformation viscosity of the Shear-thinning fluid, P_y is the plastic limit of the fluid.

➢ *The Modified Fundamental Equations are [24].*

$$\frac{\partial u'}{\partial x} + \frac{\partial v'}{\partial y'} = 0 \tag{2}$$

$$\frac{\partial u'}{\partial t'} - v_0 \frac{\partial u'}{\partial y'} = \nu_f \left(1 + \frac{1}{c}\right) \frac{\partial^2 u'}{\partial y'^2} + g\dot{\beta}_t (T - T_0) + g\dot{\beta}_c (C - C_0) - \frac{\sigma_f B_0^2 u'}{\rho_f} - \nu_f \left(1 + \frac{1}{c}\right) \frac{u'}{K} - F^* u'^2 \tag{3}$$

$$\frac{\partial T}{\partial t'} - v_0 \frac{\partial T}{\partial y'} = \frac{k_f}{(\rho C_p)_f} \frac{\partial^2 T}{\partial y'^2} + \frac{Q_0}{(\rho C_p)_f} (T_0 - T) - \frac{1}{(\rho C_p)_f} \frac{\partial q_r}{\partial y'} + \frac{\sigma_f B_0^2 u'^2}{(\rho C_p)_f}$$

$$+ \frac{\mu_f}{(\rho C_p)_f} \left(1 + \frac{1}{c}\right) \left(\frac{\partial u'}{\partial y'}\right)^2 + \frac{\mu_f}{(\rho C_p)_f} \left(1 + \frac{1}{c}\right) \frac{u'^2}{K} + \tau \left[D_B \frac{\partial C}{\partial y} \frac{\partial T}{\partial y} + \frac{D_T}{T_m} \left(\frac{\partial T}{\partial y}\right)^2 \right] \tag{4}$$

$$\frac{\partial C}{\partial t} - v_0 \frac{\partial C}{\partial y} = D_B \frac{\partial^2 C}{\partial y^2} + \frac{D_T}{T_m} \left(\frac{\partial^2 T}{\partial y^2}\right) \tag{5}$$

➢ *With Initial Condition*

$$u'(t', y') = 0, T(t', y') = 0, C(t', y') = 0 \ \ at \ \ t' = 0 \tag{6}$$

➢ *For Sparse Flow with Temperature Jump, the Suitable Interface Condition can Written as*

$$u'(t', y') = \frac{2-\xi}{\xi}\gamma\frac{\partial u'}{\partial y'} \tag{7}$$

$$T(t', y') = T_1 + T_2\cos(\omega t) + \frac{2-\sigma_t}{\sigma_t}\frac{2\varphi}{\varphi+1}\frac{\gamma}{\Pr}\frac{\partial T}{\partial y'},\ y' = -h \quad at\ \ t' > 0 \tag{8}$$

$$C(t', y') = C_1 + C_2\cos(\omega t) + k_c\frac{\partial C}{\partial y'} \quad ,\ \ y' = -h \quad at \quad t' > 0$$

➢ *The Fixed Interface with Constant Temperature Condition gives*

$$u'(t', y') = 0, T(t', y') = T_1 + T_2\cos(\omega t), \quad y' = h \quad at \quad t' > 0$$

$$C(t', y') = C_1 + C_2\cos(\omega t), \quad y' = h \quad at \quad t' > 0 \tag{9}$$

➢ *By using Roseland Approximation, the Radiative Thermal Emission term is given by*

$$q_r = -\frac{4\gamma'}{3\alpha'}\frac{\partial T^4}{\partial y'} \tag{10}$$

Where γ' and α' are stefan Boltzman constant and Roseland mean absorptivity. Presuming the difference with the flow is infinitesimal such that T^4 can be expressed as a temperature-dependent linear function. It can be acheived by expansion of T^4 in a Taylor series about T and ignoring the higher order terms, we have

$$\dot{T}^4 = (4T_1)^3 T - 3T_1^4 \tag{11}$$

➢ *Substituting Equation (9) and (10) into Equation (3) gives*

$$\frac{\partial T}{\partial t'} - v_0\frac{\partial T}{\partial y'} = \frac{k_f}{(\rho C_p)_f}\frac{\partial^2 T}{\partial y'^2} + \frac{Q_0}{(\rho C_p)_f}(T_0 - T) - \frac{16\gamma' T_1^3\partial^2 T}{3\alpha'\partial y'^2} + \frac{\sigma_f B_0^2 u'^2}{(\rho C_p)_f}$$

$$+\frac{\mu_f}{(\rho C_p)_f}\left(1+\frac{1}{c}\right)\left(\frac{\partial u'}{\partial y'}\right)^2 + \frac{\mu_f}{(\rho C_p)_f}\left(1+\frac{1}{c}\right)\frac{u'^2}{K} + \tau\left[D_B\frac{\partial C}{\partial y}\frac{\partial T}{\partial y} + \frac{D_T}{T_m}\left(\frac{\partial T}{\partial y}\right)^2\right] \tag{12}$$

III. MODEL TRANSFORMATION

By solving equations (2) to (12), then equations (13) to (15) were employed to separate the velocity, temperature and concentration into steady and unsteady part, correspondingly according to [24], as follows:

$$u'(t', y') = \frac{h^2}{\nu}\left((T_1 - T_0)A(y) + T_2 B(y)e^{i\omega t}\right) \tag{13}$$

$$T'(t', y') = T_0 + (T_1 - T_0)F(y) + T_2 G(y)e^{i\omega t} \tag{14}$$

$$C'(t', y') = C_0 + (C_1 - C_0)M(y) + C_2 Z(y)e^{i\omega t} \tag{15}$$

Wherein A(y), F(y), M(y) depicts the steady parts and B(y), G(y), Z(y) the non-steady parts of the velocity, temperature and concentration, correspondingly. The dimensionless variables used are:

$$y=\frac{y'}{h}\ ,\ S_t=\frac{i\omega}{\nu}\ ,\ \ P_r=\frac{k_f}{\left(\rho C_p\right)_f\nu_f}\ ,\ \delta=\frac{Q_0}{k_f}\ ,\ c=\frac{\mu_B\sqrt{2\pi}}{P_y}\ ,\ K_n=\frac{\lambda}{h}\left(\frac{2-\sigma_t}{\sigma_t}\right)\frac{2\varphi}{\varphi+1}$$

$$Da=\frac{k}{h^2}\ ,\ \gamma=\frac{(2-\xi)\lambda}{\xi h}\ ,\ H=\frac{\sigma_f B_0{}^2}{\mu_f}\ ,\ \beta=\frac{1}{Da}\ ,\ N=\frac{4\sigma T_1^3}{\alpha k_f}\ ,\ E_c=\frac{h^4}{C_p\nu_f}\rho\left(T_1-T_0\right)$$

$$,\ Nb=\frac{\tau D_B\left(C_1-C_0\right)}{\nu_f}\ ,\ Nt=\frac{\tau D_T\left(T_1-T_0\right)}{T_m\nu_f}$$

$$\alpha_f=\frac{k_f}{\left(\rho C_p\right)_f}\ ,\ Le=\frac{\alpha_f}{D_B}\ ,\ \delta_1=\frac{k_c\,h^2}{\nu_f}\ ,\ S=\frac{v_0}{\nu_f}\ ,\ \lambda=\frac{g\beta_t}{h^2}\ ,\ Q_1=\frac{\beta_c\left(C_1-C_0\right)}{\beta_t\left(T_1-T_0\right)}\ `Q_2=\frac{\beta_c C_2}{\beta_t T_2}\ ,\ Sc=\frac{v_0}{D_B}\ ,$$

$$\left(\frac{Nt}{Nb}\right)=\frac{D_T\left(T_1-T_2\right)}{T_m D_B\left(C_1-C_2\right)}\ \ , \tag{16}$$

Applying equation (13) to (15) into the equations (3) to (5) and taking the order of $e^{i\omega t}$, non-linear coupled ordinary differential equations was obtained as:

$$\left(1+\frac{1}{c}\right)A''(y)+SA'(y)-\left(H^2+\left(1+\frac{1}{c}\right)\beta\right)A(y)+\lambda\left(F(y)+Q_1M(y)\right)-Fc\left(A(y)\right)^2=0 \tag{17}$$

$$\left(1+\frac{4}{3}N\right)F''(y)+\Pr SF'(y)+\Pr\left(NbM'(y)+NtF'(y)\right)F'(y)+\delta F(y)$$

$$+\Pr Ec\left(H^2+\beta\left(1+\frac{1}{c}\right)\right)\left(A(y)\right)^2+\Pr Ec\left(A'(y)\right)^2=0 \tag{18}$$

$$\left(1+\frac{1}{c}\right)B''(y)+SB'(y)-\left(S_t+H^2+\left(1+\frac{1}{c}\right)\beta\right)B(y)+\lambda\left(G(y)+Q_2Z(y)\right)-2Fc\cdot A(y)B(y)=0 \tag{19}$$

$$\left(1+\frac{4}{3}N\right)G''(y)+\Pr SG'(y)+2Nt\Pr G'(y)+Nb\Pr\left(M'(y)G'(y)+Q_3F'(y)Z'(y)\right)-\left(\Pr S_t+\delta\right)G(y)$$

$$+2\Pr Ec\left(H^2+\left(1+\frac{1}{c}\right)\beta\right)A(y)B(y)+2\Pr Ec\left(1+\frac{1}{c}\right)A'(y)B'(y)=0 \tag{20}$$

$$M''(y)+ScM'(y)+\left(\frac{N_t}{N_b}\right)F''(y)=0 \tag{21}$$

$$Z''(y)+Sc(SZ'(y)-S_tZ(y))+\left(\frac{Nt}{Nb}\right)G''(y)=0 \tag{22}$$

➢ *The Equations Underwent the Specified Boundary Conditions Outlined in Equation (23)*

$$A(-1)=\gamma A'(-1),\ A(1)=0$$

$$F(-1)=1+\frac{K_n}{P_r}F'(-1),\ F(1)=1$$

$$M(-1)=1+\delta_1 M'(-1),\ M(1)=1$$

$$B(-1)=\gamma B'(-1),\ B(1)=0$$

$$G(-1)=1+\frac{K_n}{P_r}G'(-1),\ G(1)=1$$

$$Z(-1)=1+\delta_1 Z'(-1),\ Z(1)=1 \tag{23}$$

The coefficient of skin friction $C_f=\left(1+\frac{1}{c}\right)\frac{dB(y)}{dy}$, the heat transfer rate $Nu=\left(1+\frac{4}{3}N\right)\frac{dG(y)}{dy}$ and the mass transfer rate $Sh=\frac{dZ(y)}{dy}$ at the walls .

IV. NUMERICAL PROCEDURE

The system of second order non-linear univariate equations (17) to (22) is transformed into a set of first-order univariate equation by substitution;

$$\text{Let } d_1=A,\ d_2=A',\ d_3=B,\ d_4=B',\ d_5=F,\ d_6=F',\ d_7=G,\ d_8=G',\ d_9=M,\ d_{10}=M',\ d_{11}=Z,\ d_{12}=Z' \tag{24}$$

➢ *Substituting Equation (24) into Equations (17) to (22) give the Required set of First-Order Differential Equations as;*

$$d_2'=\frac{\left(H^2+\beta\left(1+\frac{1}{c}\right)\right)d_1-\lambda(d_5+Q_1d_9)-Sd_2}{\left(1+\frac{1}{c}\right)} \tag{25}$$

$$d_6'=\frac{-1}{\left(1+\frac{4}{3}N\right)}\left(\Pr Sd_6+\delta d_5+\Pr Ec\left(H^2+\beta\left(1+\frac{1}{c}\right)\right)d_1^2+\Pr Ecd_2^2+\Pr(Nbd_{10}+\Pr Ntd_6)d_6\right) \tag{26}$$

$$d_{10}'=-Scd_{10}-\left(\frac{Nt}{Nb}\right)d_6' \tag{27}$$

$$d_4'=\frac{\left(S_t+H^2+\beta\left(1+\frac{1}{c}\right)\right)d_3-\lambda(d_7+Q_2d_{11})-Sd_4}{\left(1+\frac{1}{c}\right)} \tag{28}$$

$$d_8'=\frac{-1}{\left(1+\frac{4}{3}N\right)}\left(\begin{array}{l}\Pr Sd_8-\Pr S_td_7-\delta d_7+2H^2\Pr Ecd_1d_3+2\Pr Ec\left(1+\frac{1}{c}\right)d_2d_4\\+2\Pr Ec\beta\left(1+\frac{1}{c}\right)d_1d_3+Nb\Pr(d_8d_{10}+Q_3d_6d_{12})+2\Pr Ntd_6d_8\end{array}\right) \tag{29}$$

$$d'_{12} = -Sc\left(Sd_{12} - S_t d_{11}\right)d_{10} - \left(\frac{Nt}{Nb}\right)d'_8 \tag{30}$$

- *Subject to the Boundary Conditions;*

$$d_1(-1) = \gamma d_2(-1),\ d_1(1) = 0,\ d_5(-1) = 1 + \frac{kn}{\Pr} d_6(-1),\ d_5(1) = 1,\ d_9(-1) = 1 + \delta_1 d_{10}(-1),\ d_9(1) = 1$$

$$d_3(-1) = \gamma d_4(-1),\ d_3(1) = 0,\ d_7(-1) = 1 + \frac{kn}{\Pr} d_8(-1),\ d_7(1) = 1,$$

$$d_{11}(-1) = 1 + \delta_1 d_{12}(-1),\ d_{11}(1) = 1 \tag{31}$$

The shooting technique is utilized to guess the unknown points $d_2(-1) = q_1, d_4(-1) = q_2, d_6(-1) = q_3, d_8(-1) = q_4,$ $d_{10}(-1) = q_5, d_{12}(-1) = q_6$ until the boundary condition is satisfied. The fourth-order Runge-Kutta integration approach was adopted to solve the resultant differential equations, and numerical computations are carried out with the Maple 18 software package. To validate the correctness of the results presented and to determine the accuracy of the numerical method adopted, a comparison of result with the existing one is carried out as presented in Table 1

Table 1 Comparison of Results for $G(y)$ with Previous Works for: S =1, St =1, β = 0, H = 0, δ =1, $\Pr = 1$, $N = 15$, $Kn = 0$, $\gamma = 0$, $Ec = 0$, $\lambda = 0$, $Q_1 = 0$.

y	Titiloye(2018)	Obalalu (2020)	Present work
-1.0	0.999999	0.999999	1.000000
-0.8	0.799521	0.799521	0.799521
-0.6	0.685677	0.685677	0.685677
-0.4	0.626398	0.626398	0.626398
-0.2	0.605794	0.605794	0.605794
0	0.602555	0.602555	0.602555
0.2	0.646716	0.646716	0.646716
0.4	0.700614	0.700614	0.700614
0.6	0.775963	0.775963	0.775963
0.8	0.874578	0.874578	0.874578
1.0	0.999999	0.999999	1.000000

V. RESULTS AND DISCUSSION

In this section, the significance of various thermophysical dynamical terms on unsteady flow regimes was presented with the help of plots. It can be observed from Table 2, that the skin friction increased whenever radiation and thermophoresis dynamical term gained values but decreased with an upsurge in magnetic and permeability dynamical terms. Also an upsurge in thermophoresis decreased the Nusselt number while it diminished with an upsurge in radiation and magnetic dynamical terms. Sherwood number increased with an upsurge in thermophoresis but diminished with an upsurge in radiation and porous dynamical terms.

Table 2 Effect of Different Thermo Physical Dynamical Terms on the Shear Stress, the Heat Transfer rate and the rate of mass Transfer at the Surface of the Plate for $Kn = 0.005, S_t = \delta = Sc = \gamma = 1.0,\ c = Q_1 = Q_2 = 0.1,\ \Pr = 0.71.$

c	Ec	H	N	S	Nb	Nt	β	(C_f)	-(Nu)	-(Sh)
0.1	0.6	1.5	2	0.2	0.2	0.2	1.0	0.029702	0.322713	0.542301
1.5	0.6	1.5	2	0.2	0.2	0.2	1.0	0.121321	0.302734	0.558802
2.0	0.6	1.5	2	0.2	0.2	0.2	1.0	0.128413	0.301223	0.559933
0.1	2.0	1.5	2	0.2	0.2	0.2	1.0	0.031840	0.073231	0.747634
0.1	4.0	1.5	2	0.2	0.2	0.2	1.0	0.035302	0.361402	1.104721
0.1	0.6	2.5	2	0.2	0.2	0.2	1.0	0.026214	0.309012	0.553622
0.1	0.6	5.0	2	0.2	0.2	0.2	1.0	0.016830	0.272743	0.583443
0.1	0.6	1.5	7	0.2	0.2	0.2	1.0	0.031421	0.119741	0.709544

0.1	0.6	1.5	8	0.2	0.2	0.2	1.0	0.031511	0.106422	0.720412
0.1	0.6	1.5	2	1.0	0.2	0.2	1.0	0.029843	0.338323	0.651914
0.1	0.6	1.5	2	3.5	0.2	0.2	1.0	0.030012	0.386211	0.900512
0.1	0.6	1.5	2	0.2	0.4	0.2	1.0	0.029630	0.322902	0.674533
0.1	0.6	1.5	2	0.2	0.6	0.2	1.0	0.029602	0.322803	0.718620
0.1	0.6	1.5	2	0.2	0.2	0.4	1.0	0.029921	0.330611	0.262601
0.1	0.6	1.5	2	0.2	0.2	0.6	1.0	0.030133	0.338431	0.032413
0.1	0.6	1.5	2	0.2	0.2	0.2	2.0	0.021714	0.291530	0.567922
0.1	0.6	1.5	2	0.2	0.2	0.2	3.0	0.017141	0.273642	0.582634

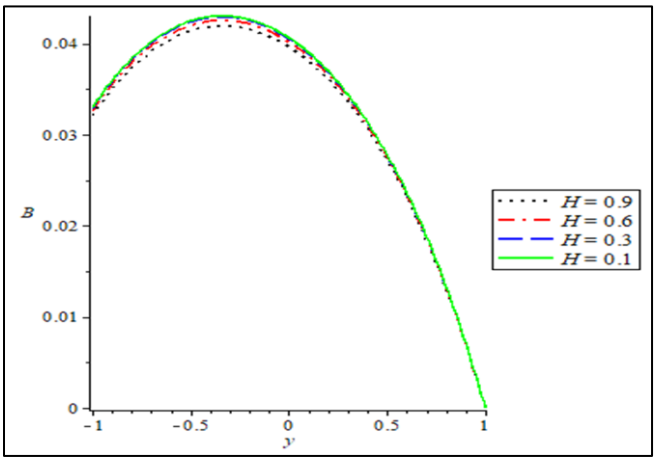

Fig 1 Influence of Varying Hartmann Number on Flow Plot

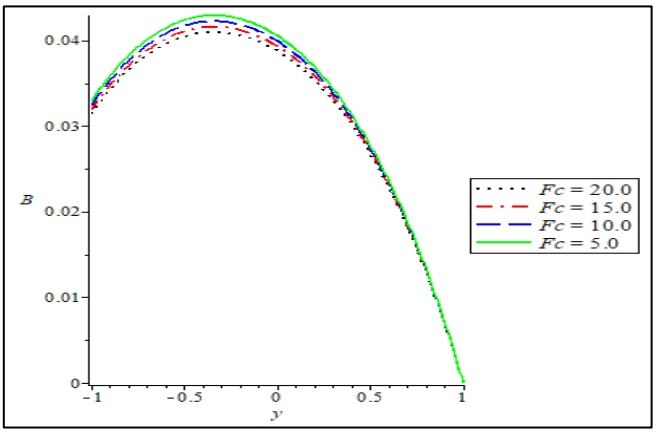

Fig 4 Significance of Varying Forchheimer Dynamical Term on Flow Plot

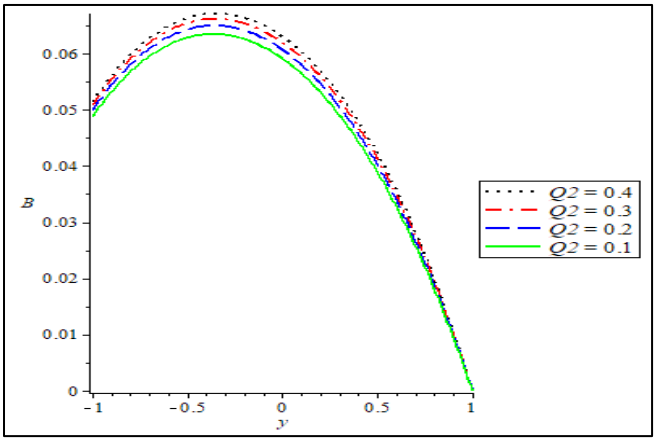

Fig 2 Significance of Varying Buoyancy ratio on Flow Plot

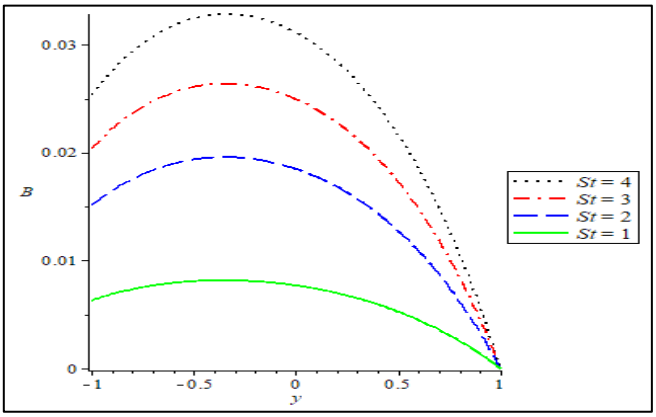

Fig 5 Significance of Varying Strouhal Number on Flow rate Plot

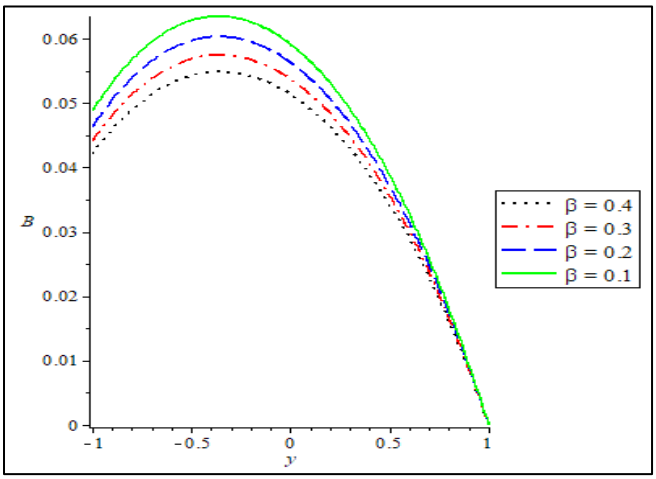

Fig 3 Significance of Varying Porous Parameter on Flow Plot

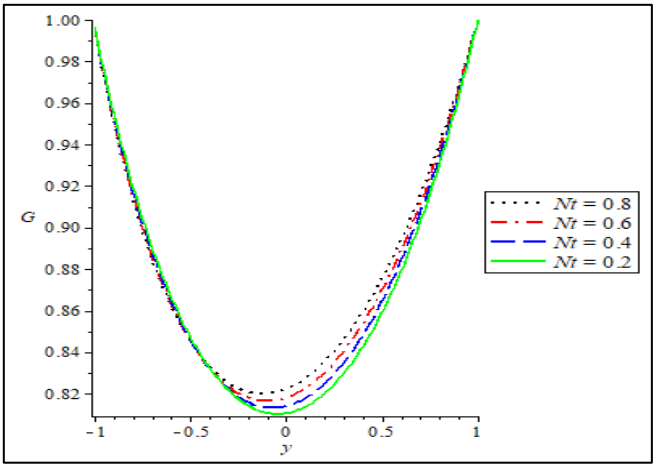

Fig 6 Thermal Measurement Profile for Various Thermophoresis Parameter

ISSN No:-2456-2165

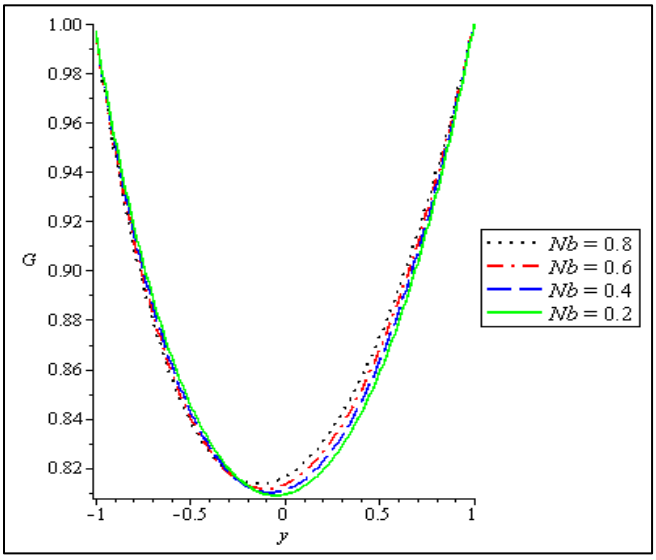

Fig 7 Thermal Measurement Profile for Various Brownian Parameter

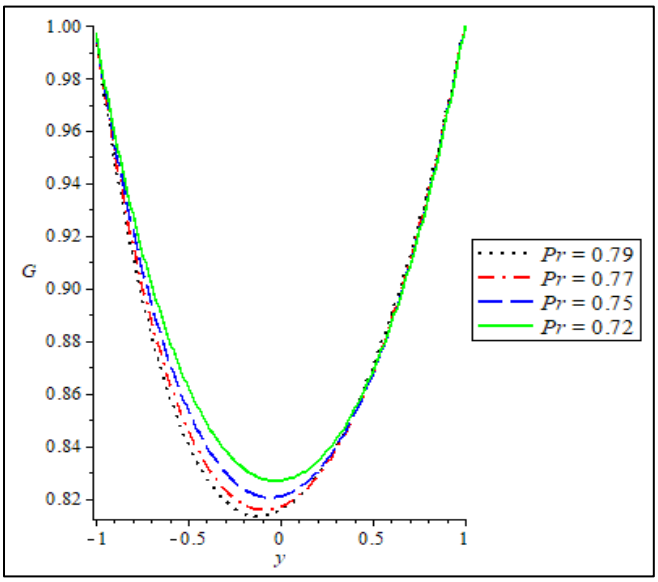

Fig 8 Thermal Measurement Profile for Various Prandtl Number

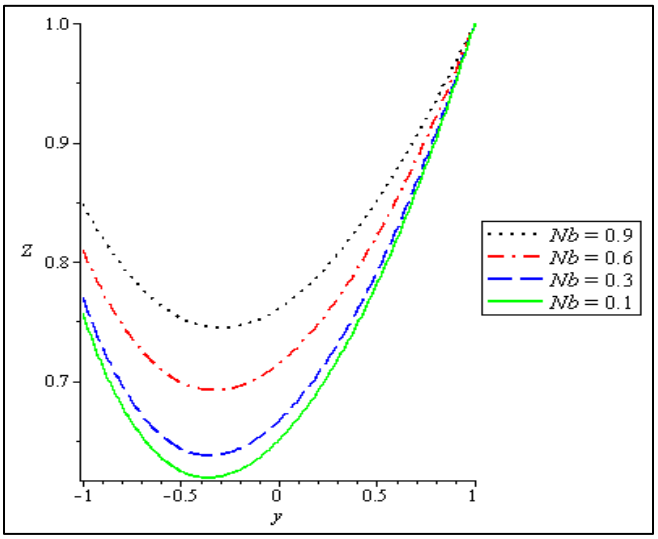

Fig 9 Concentration Graph for Various Brownian Parameter

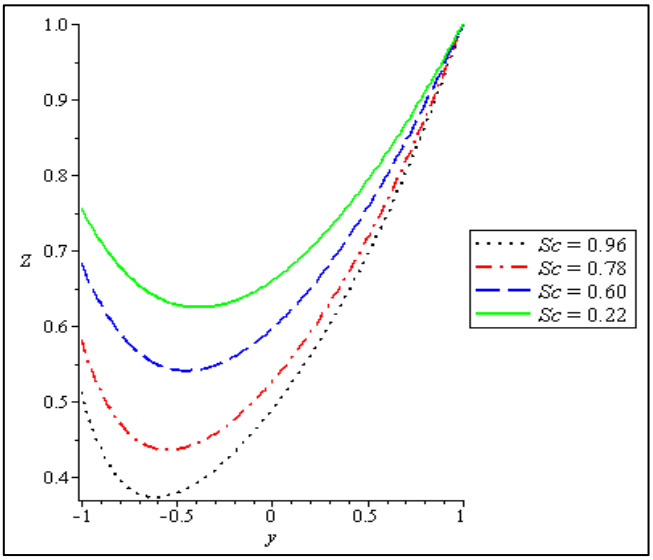

Fig 10 Concentration Profile for Varying Schmidt Number

Figure 1-10 display the response of fluid flow rate, thermal measurement and mass transfer graphs against space for the variation of sensitivity parameters in the unsteady flow regime.

For different Hartmann numbers, the velocity curve is displayed in Figure 1. The standard component of the velocity profile in the flow zone decreases as the Hartmann number improves. It is logical to assume that an essentially higher Hartmann number results in higher Lorentz forces connected to magnetic fields. The fluid is met with resistance as it passes through the channel as a result of the strong Lorentz forces. As a result, when the Hartmann number improves, the intensity of the velocity field reduced.

Figure 2 illustrates how buoyancy ratio affects velocity field. It follows that a rise in the buoyancy ratio also raises the fluid's thermal diffusivity, which boosts flow. The velocity field is shown in Figure 3 to be affected by the porosity parameter. The velocity of the flow has been found to decrease as the porosity dynamical term improves. Figure 4 depicts how the Forchheimer parameter affects velocity. It was found that as the value of the Forchheimer dynamical term improves, the fluid flow reduced. The increase in the Forchheimer parameter indicates that the system is producing the resistive forces. This causes the fluid's motion to slow down, which lowers the velocity. The significance of strouhal number on the velocity plot is seen in Figure 5. It has been found that increasing strouhal dynamical term increases flow velocity. The significance of thermophoresis and Brownian motion dynamical terms on the thermal profile is depicted in Figure 6 and Figure 7. Notably, an augmentation in the thermophoresis and Brownian dynamical terms corresponds to an elevation in the nusselt number. From a physical perspective, as the intensity of Brownian motion increases, it facilitates the efficient movement of nanoparticles from the walls to the fluid, consequently leading to an improvement in fluid’s thermal measurement.

The significance of the Prandtl number on thermal measurement is depicted through Figure 8. The results indicate that an augmentation in the Prandtl number corresponds to a reduction in the thermal measurement profile. This observation implies a decline in the fluid's thermal conductance, as evidenced by the linked decrease in temperature. Figure 9 showcase the significance of Brownian motion parameter on the periodic concentration of nanoparticles. Upon close examination, it becomes apparent that an escalation in the Brownian dynamical term resulted in the improvement of nanoparticle concentration. This heightened oscillation can be attributed to the efficient displacement of nanoparticles from the left boundary into the fluid. In Figure 10, the impact of altering the Schmidt number on the periodic concentration of nanoparticles is illustrated. An upsurge in the Schmidt number correlates to a reduction in concentration. This phenomenon can be attributed to the inherent nature of the Schmidt number, which signifies the interplay between diffusivity and viscous forces. Consequently, a higher Schmidt number led to a reduction in species concentration.

VI. CONCLUSION

A mathematical framework that examined the unsteady mixed heat-driven flow of Casson nanofluid within vertical permeable channel, incorporating slip and temperature jump constraints is presented. The study delves into the significant of controlling dynamical terms on fluid flow, heat and mass transfer characteristics. Flow features are displayed through graphical representations and thoroughly elucidated. The ensuing conclusions are synopsized as follows:

- There was enhancement of flow rate with an augmentation in the buoyancy dynamical term and strouhal number whereas it declines with an escalation in the magnetic dynamical term, porous dynamical term and Forchheimer dynamical term.
- Thermal distribution escalates with a rise in thermophoresis dynamical term and Brownian dynamical term while it diminishes with an upsurge in the Prandtl number.
- Concentration distribution reduces with an escalation in the Schmidt number while it improves with an upsurge in the Brownian motion dynamical term.

REFERENCES

[1]. Rafique, K., Anwar, M.I., Misiran, M., Khan, I., Baleanu, D., Nisar, K.S., Sherif, E.M. and Seikh, A. (2020). Hydromagnetic flow of micropolar nanofluid, *Symmetry* 12, 251.

[2]. Musa, A.M., Verdiana, G.M., Eunice, W.M. and Makungu, N.J. (2019). Unsteady MHD flow of nanofluid with variable properties over a stretching sheet in the presence of thermal radiation and chemical reaction, *International Journal of Mathematics and Mathematical Sciences*, 1-14.

[3]. Rafique, K., Anwar, M.I. and Misiran, M. (2019). Numerical study on micropolar nanofluid flow over an inclined surface by means of Keller-box. *Asian J. Probab. Stat*, 4, 1-21.

[4]. Singh, J., Vishalakshi, A.B., Mahabaleshwar, U. S and Bognar, G (2022). MHD Casson fluid flow with Navier's and second order slip due to a perforated stretching on shrinking sheet. *Journal.pone*, 17(11): e0276870.

[5]. Radha, G., Reddy, N.B and Gangadhor, K (2017). Slip flow of Casson fluid with variable thermophysical properties along exponentially stretching sheet under convective heating. *International Journal of Mechanics and Solids*. 12(2), (2017), Pp 235-256.

[6]. Arthur, E.M., Seini, I.Y. and Bortteir, L.B. (2015). Analysis of Casson fluid flow over a vertical porous surface with chemical reaction in the presence of magnetic field. *Journal of Applied Mathematics and Physics*, 3(2015), 713-723.

[7]. Buongiorno, J. (2006).Convective transport in nanofluids, *Journal of Heat Transfer*, 128, 240-250.

[8]. Motsumi, T.G and Makinde, O.D. (2012). Effects of thermal radiation and viscous dissipation on boundary layer flow of nanofluids over a permeable moving flat plate. *Phys. Scr.* 86(4). DOI:10.1088/0031-8949/86/04/045003.

[9]. Das, K., Duari, P.R. and Kundu, P.K (2014). Nanofluid flow over an unsteady stretching surface in the presence of thermal radiation, *Alexandria Engineering Journal*, 53, 737-745.

[10]. Uddin, M.J., Beg, O.A., and Amin, N. (2014). Hydromagnetic transport phenomena from a stretching or shrinking nonlinear nanomaterial sheet with Navier slip and convective heating: a model for bio-nano-materials processing. *Journal of Magnetism and Magnetic Materials*, 368, 252-261.

[11]. El-dawy, H.S.A.and Gorla R.S.R. (2019). Effects of nanoparticles on Non-Darcy mixed convective heat transfer in nanofluids over a shrinking and stretching wedge, *Applied Computational Mathematics*, 8(4), 70-74.

[12]. Wang, J., Mustafa, Z., Siddique, I., Ajmal, M., Jaradat, M.M., Rehman, S.U. and Ali, H.M. (2022).Computational analysis for bio-convection of microorganisms in Prandtl nanofluid Darcy-Forchheimer flow across an inclined sheet. *Nanomaterials*, 12(11), 1791.

[13]. Sayed, E.A. and Fathy, M. (2022). Numerical study of flow and heat transfer of a nanofluid past a vertical cone. *Case Studies in thermal Engineering*, 34, 102038.

[14]. Kamram, A., Hussain, S., Sagheer, M. and Akmal, N (2017). A numerical study of magnetohydrodynamics flow in Casson nanofluid combined with joule heating and slip boundary conditions. www.journals.elsevier.com/results-in-physics(2017), 3037-3048.

[15]. Oyelakin , I.S., Modal, S and Sibanda, P (2016). Unsteady Casson nanofluid flow over a stretching sheet with thermal radiation, convective and slip boundary conditions. *Alexandria Engineering Journal, AEJ journal* (2016), 55, 1025-1035.
[16]. Gbadeyan, J.A., Titiloye, E.O. and Adeosun, A.T. (2019). Effect of variable thermal conductivity and viscosity on Casson nanofluid flow with convective heating and velocity slip. *Helion* 6(2020), 2405-8440.
[17]. Lund, L.A., Omar, Z., Sherif, E.S.M and Abdo, H.S (2020). Stability analysis of the magnetized Casson nanofluid propagating through an exponentially shrinking/stretching plate: Dual solutions. *Symmetry.www.mdps.com/journal/symmetry (2020)*, 12, 1162-1181.
[18]. Sharma, S. (2022). MHD boundary layer flow past an exponentially stretching sheet with Darcy-Forchheimer flow of nanofluids. *Indian Journal of Science and Technology*, 15(33), 1594-1604.
[19]. Rashad, A.M.,Nafe, M.A. and Eisa, D.A. (2022). Heat generation and thermal radiation impacts on flow of magnetic Eyring-Powell hybrid nanofluid in a porous medium. *Arabian Journal for Science and Engineering*, 1-14.
[20]. Jafar, A.B., Shafie, S. and Ullah, I. (2020). MHD radiative nanofluid flow induced by a non-Linear stretching sheet in a porous medium. *Heliyon*, 6 (6), 04201.
[21]. Rauf, A., Abbas, Z. and Shehzad, S.A. (2019). Chemically reactive hydromagnetic flow over a stretching oscillatory rotating disk with thermal radiation and heat source/sink: A numerical study. *Heat Transfer Research*, 50 (15):360-386.
[22]. Sivaraj, R and Benazir, A.J (2015). Unsteady magnetohydrodynamics mixed convective oscillatory flow of Casson fluid in a porous asymmetric wavy channel. Special topics and reviews in porous media: *An International Journal*, 6 (3): 267-281.
[23]. Khaled, A.R and Vafai, K. (2004). The effect of the slip condition on Stokes and Couette flows due to an oscillating wall: exact solutions. *International Journal of Non-Linear Mechanics*, 39 (5): 795-809.
[24]. Obalalu, A.M., Ajala, O.A., Adeosun, A.T., Wahaab, F.A., Aliu, O and Adebayo, L.L (2020). Natural convective non-Newtonian Casson fluid flow in a porous medium with slip and temperature jump boundary conditions. *Petroleum and Coal Open Access Journal*. 62 (4):1532-1545.